Structural State and Redox Behavior of Framework Co(II) in CoIST-2: A Novel Cobalt-Substituted Aluminophosphate with AEN Topology

C. Borges,[†] M. F. Ribeiro,[†] C. Henriques,[†] J. P. Lourenço,[‡] D. M. Murphy,[§] A. Louati,[||] and Z. Gabelica*,[⊥]

Departamento de Engenharia Química, Instituto Superior Técnico, Av. Rovisco Pais, P-1049-001 Lisboa, Portugal, Faculdade de Ciências e Tecnologia, Departamento de Química e Bioquímica, Universidade do Algarve, Campus de Gambelas, P-8000-117 Faro, Portugal, Department of Chemistry, Cardiff University, P.O. Box 912, Cardiff CF10 3TB, United Kingdom, Laboratoire d'Electrochimie Analytique, ENSCMu, Université de Haute Alsace, 3, rue A. Werner, F-68093 Mulhouse Cedex, France, and Groupe Sécurité et Ecologie Chimiques, ENSCMu, Université de Haute Alsace, 3, rue A. Werner, F-68093 Mulhouse Cedex, France

Received: October 28, 2003; In Final Form: April 7, 2004

A highly crystalline cobalt-substituted aluminophosphate with an AEN topology, labeled CoIST-2, has been synthesized and characterized by powder XRD, TG/DSC, diffuse reflectance UV−vis spectroscopy, FTIR, EPR spectroscopy, and cyclic voltammetry. Both water and methylamine were shown to play a complementary role as dual template and space-filling agents during the hydrothermal synthesis of this material. The spectroscopic (EPR, UV−vis, and FTIR) and electrochemical characterization of the as-synthesized and calcined CoIST-2 material revealed the presence of two structurally different Co(II) species incorporated in its crystalline framework. The redox behavior and acidity was found to be different for these two Co(II) species. While one of these cobalt species corresponded to Brönsted Co(OH)P acid sites, the other seemed to be associated with the presence of Lewis acid sites (Co□P type species). UV−vis spectra, typical of divalent cobalt in tetrahedral coordination, along with FTIR, demonstrated that only a fraction of the Co(II) ions undergo a reversible oxidative process after calcination in air and that some extraframework Co_xO_y type species are also generated through oxidation. The presence of divalent Co(II) in a slightly distorted tetrahedral coordination, both in the as-synthesized and calcined phase, was also detected with use of EPR data. The electrochemical oxidation of the two different framework Co(II) species and their further reduction could be evaluated semiquantitatively by cyclic voltammetry. The redox ability of CoIST-2 was also compared with that of two other cobalt-substituted aluminophosphates involving different pore structures, namely CoAPO-40 and CoAPO-37, by using FTIR of adsorbed NO. It was found that the most readily oxidized ions were present in the more dense AEN topology, followed by the more open AFR and FAU structures, thereby emphasizing how the redox properties of transition metal ions in porous aluminophosphates are intimately linked to both the structure type/density of the host lattice and framework positions of the heteroelement.

Introduction

MeAPO's, in which transition metal ions are incorporated into the aluminophosphate-based framework, are of great interest for possible catalytic applications.[1−4] The incorporation of a divalent ion into the framework, substituting for a trivalent aluminum ion, results in the generation of an acid site if the network negative charge is compensated by a proton. In addition, the ability of the transition metal ions to change their oxidation state and/or coordination toward the reactants also provides catalytic sites that can assist specific redox reactions. The incorporation of cobalt into aluminophosphate materials has been claimed for a variety of structures but the coordination and redox properties of the framework cobalt ions are still controversial and seem to be dependent on the nature of the structure itself.[5−10] These metal ion containing systems have also been extensively investigated specifically due to their promising catalytic behavior in the oxidation of organic compounds and in the removal of NOx compounds.[11,12] In this respect, cobalt is interesting not only because of its promising catalytic activity, but also due to its rich spectroscopy in its divalent state.[11]

The AEN family of aluminophosphate-based materials was first reported in the literature in 1985 with the synthesis of aluminophosphate AlPO-EN3.[13] Since then, several materials with a similar structure have been synthesized by different research groups including CFSAPO-1A,[14] MSC-1,[15] GaPO-AEN,[16] JDF-2,[17] AlPO-53(A) and AlPO-53(B),[18] and UiO-12.[19] The pore structure of the calcined material (AlPO-53(B)) consists of two 8-ring channels intersecting to generate a 2D channel system with pore openings of 4.3 × 3.1 and 2.7 × 5.0 Å^2.[18−20]

Recently, our group, while studying the influence of co-templates for the synthesis of various aluminophosphate materials, had successfully synthesized a product having an XRD pattern similar to that of CFSAPO-1.[14] It was labeled IST-2.[21]

* Corresponding author. Phone: +33 3 89 33 68 94. Fax: +33 3 89 33 68 15. E-mail: z.gabelica@uha.fr.
[†] Instituto Superior Técnico.
[‡] Universidade do Algarve.
[§] Cardiff University.
[||] Laboratoire d'Electrochimie Analytique, ENSCMu, Université de Haute Alsace.
[⊥] Groupe Sécurité et Ecologie Chimiques, ENSCMu, Université de Haute Alsace.

10.1021/jp037251p CCC: $27.50
Published on Web 05/25/2004

The thorough characterization of the as-synthesized IST-2 material allowed us to conclude that its topology is closely related to that of AlPO-53(A).

Here we report the synthesis and characterization of a pure cobalt-substituted analogue of IST-2, hereafter named CoIST-2. With the exception of a framework-incorporated Cu(II)IST-2 and Cu(I)IST-2 metalloaluminophosphate,[22] the CoIST-2 material reported here is the first example of a divalent metal incorporated into the framework of an AEN-type material. The characterization presented here, in terms of the acid and redox properties of this relatively small pore material, provides a detailed contribution toward our understanding of isomorphous substitution in aluminophosphate materials by transition metal ions and more specifically by Co(II). Generally speaking this contribution offers a glimpse into the difficulties and pitfalls encountered when generalizing the versatile redox and catalytic properties of framework cobalt in various microporous aluminophosphate structures.

Experimental Section

(1) Synthesis Procedures. The preparation of CoIST-2 followed closely the optimized synthesis method for IST-2.[21] The crystallization occurred from a synthesis gel with composition Al_2O_3:P_2O_5:0.4MA:TEAOH:0.04$Co(CH_3COO)_2$:40H_2O (MA = methylamine (template) and TEAOH = tetraethylammonium hydroxide (additive)).

For the gel preparation, 3.11 g of alumina (PURAL SB, Condea) was added to diluted orthophosphoric acid (Merck, 85%) (5.84 g of acid dissolved in 9.38 g of water) and the resulting solution was homogenized for 2 h. The cobalt source (0.22 g of $Co(CH_3COO)_2 \cdot 2H_2O$, Merck, p.a. dissolved in the remaining quantity of water) was added to this suspension and the resulting gel was agitated for about 30 min; 1.59 g of methylamine (41% aq sol, Fluka) was then introduced and, after another 30 min of homogenization, 10.58 g of TEAOH (35% aq sol, Alfa) was added. The final gel was maintained under agitation for 2 h.

The gel was introduced into Teflon-lined autoclaves placed in a preheated oven at 170 °C and left to crystallize for 24 h under static conditions. The autoclaves were cooled to room temperature under running water and the products were recovered by centrifugation, washed, and dried at 80 °C overnight.

(2) Characterization. All the samples were analyzed for purity and crystallinity by X-ray powder diffraction (Rigaku diffractometer with Cu Kα radiation filtered by Ni) and by scanning electron microscopy (Hitachi F-2400 microscope). The bulk elemental analysis for P, Al, and Co was performed by using ICP while the water and methylamine contents were determined independently combining the Kjeldahl titration method and TG-DSC. Thermal analysis (combined TG-DSC) was carried out on a Setaram TGA-92 microbalance under flowing nitrogen at a heating rate of 10 °C/min. The UV−vis spectra were obtained on a Shimadzu MPC 3100 instrument equipped with an integrating sphere coated with $BaSO_4$. The spectral data were acquired in the 13000−43000 cm^{-1} range. To remove the template and run the UV−vis spectrum of the sample treated under oxidative conditions, the product was heated under an air flow at a heating rate of 5 °C/min up to 400 °C (based on the TG analysis, this temperature was sufficient to remove the template) and then maintained isothermally at that temperature for 8 h. After cooling to ambient temperature under dry nitrogen, the sample was transferred to a quartz cell and sealed to avoid contact with atmospheric moisture. The UV−vis spectrum of the sample activated under reducing conditions was obtained by treating a sample under the same conditions as described above, followed by heating under flowing H_2 at 400 °C for 8 h.

The FTIR spectra were obtained on a Thermo Nicolet Nexus spectrometer with a resolution of 4 cm^{-1}. Before recording the spectra, the self-supported wafers of precalcined samples (adopting the same conditions as described above for the UV−vis experiments) were oxidized in O_2 at 400 °C for 8 h. After the IR spectrum was recorded under these conditions, the sample was further treated under H_2 for 8 h at 400 °C and a new IR spectrum was recorded. The adsorptions of probe molecules and subsequent treatments were performed on both the oxidized and reduced samples.

For EPR measurements, a small quantity (ca. 5 mg) of the as-synthesized or calcined CoIST-2 sample was placed into a high-purity quartz EPR cell, fitted with an appropriate adaptor for connection to a vacuum manifold. The samples were evacuated to a residual pressure of 10^{-5} mbar before recording, to remove air from the cell. The EPR spectra were recorded on a CW X-band Bruker ESP 300E series spectrometer operating at 100 kHz field modulation in a Bruker ER 2210ST standard cavity. All EPR spectra were recorded at 10 K. Accurate g values were obtained with a Bruker ER 035 M NMR gaussmeter calibrated by using the perylene radical cation in concentrated H_2SO_4 ($g = 2.002569$).

The redox ability of both as-synthesized and O_2-calcined CoIST-2 was analyzed by cyclic voltammetry (CV), using modified carbon paste electrodes. Voltammetric experiments were performed on an EG&G 263 A potentiostat modulated by EG&G PAR M270 software. All measurements were carried out at ambient temperature with a conventional three-electrode configuration, consisting of a platinum wire as the auxiliary electrode, modified sample-paste carbon as the working electrode, and a saturated calomel reference electrode (SCE). Pure water (18 MΩ cm, Millipore Milli-Qplus) was used throughout. Potassium chloride (Fluka, Puriss p.a.) was used as supporting electrolyte. The working electrode was constructed by using the following homemade procedure: The main part of the carbon paste electrode, consisting of a Teflon rod (of 1 cm external diameter) filled with the carbon paste and a glassy carbon rod (of 3 mm diameter), was inserted into the other end of the electrode to make the electrical contact. The modified sample−paraffin oil−carbon powder paste was prepared by thoroughly admixing in a mortar the desired amount of sample (typically 20−25 mg) with respectively 60−55 mg of carbon. Paraffin oil (35−40 μL) was then added until a homogeneous paste was obtained. The paste was packed into the electrode and a fresh surface was rapidly generated through rolling out a small plug of the paste with the glassy carbon rod. The plug was subsequently scrapped off and smoothed with a piece of white paper so as to obtain a homogeneous and uniform electrode surface.

Results and Discussion

(1) Purity and Framework Composition. The synthesis procedure described above yielded pure, highly crystalline CoIST-2, as shown by XRD powder diffraction (Figure 1) and SEM (Figure 2). The XRD powder pattern resembles that of aluminophosphates having the AEN framework type[23] and, more specifically, the pattern of AlPO-53(A),[18] confirming that the two topologies are very closely related. The air-calcined CoIST-2 exhibited a new structure (XRD pattern not shown here) that is actually analogous to that of AlPO-53(B) (the calcined AlPO-53(A)),[18] thereby confirming the AEN topology for CoIST-2.

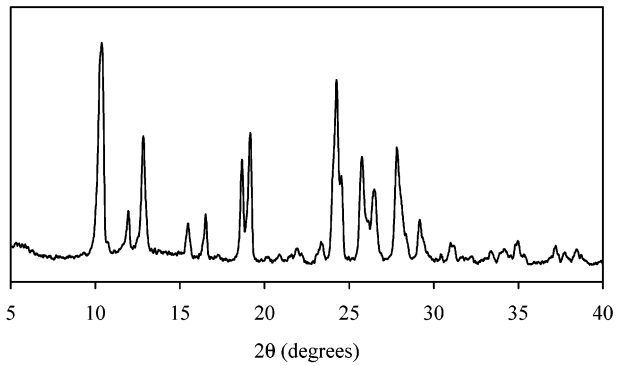

Figure 1. XRD pattern of CoIST-2.

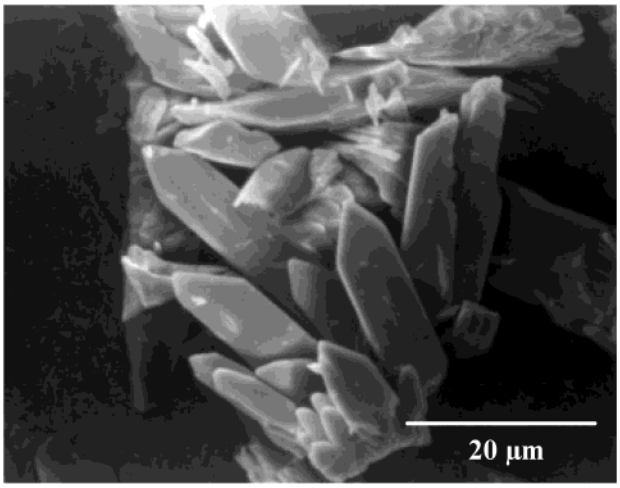

Figure 2. SEM micrograph of CoIST-2.

TABLE 1: Unit Cell Parameters of IST-2 and CoIST-2

sample	*a* (Å)	*b* (Å)	*c* (Å)	*V* (Å^3)
IST-2	10.269	13.951	16.978	2429.949
CoIST-2	10.324	13.663	17.369	2450.072

The increase of the cell volume with respect to the cell characterizing the pure aluminophosphate IST-2 synthesized under similar conditions[21] (assuming an orthorhombic system) (Table 1) is also consistent with the isomorphous substitution of cobalt(II) (4-coordinate tetrahedral ionic radius; 0.72 Å) for aluminum (tetrahedral ionic radius: 0.59 Å). Therefore, assuming cobalt incorporation and using the bulk analytical data, the framework composition of one unit cell is as follows: $Al_{23.2}P_{24}Co_{0.8}O_{96}$ or $(Co_{0.02}Al_{0.48}P_{0.50})O_2$. As discussed in detail later, the UV−vis data do not reveal any octahedral Co(II) species, and we may therefore assume that all the tetrahedral Co(II) species are true framework species, since extraframework tetrahedral Co(II) is very unlikely to occur. This assumption is further confirmed by the EPR results (as discussed later).

The TG/DSC analysis (Figure 3) first shows a progressive weight loss between 50 and about 250 °C (about 1%), which is readily attributed to the loss of some residual physisorbed water. Another sharp weight loss (about 12.2%) was observed between 250 and 350 °C. This step loss and the corresponding sharp endotherm (Figure 3) could reflect a straightforward degradation of the template, which, as in the IST-2 structure, would be exclusively methylamine even though TEAOH was also added during synthesis. The actual role of TEA is to indirectly stabilize the IST-2 topology, as discussed in a subsequent paper.[21] Indeed, IST-2 was systematically found to be 100% crystalline in the presence of TEA while amorphous aluminophosphate contaminants were found admixed with IST-2 when TEA was absent. The fact that TEA^+ ions were never found incorporated in the as-synthesized IST-2 phase was interpreted by assuming that these cations would rather interact with side formed $Al_xP_yO_z^{w-}$ oligomeric species in solution and form soluble complexes or associations with them. Conversely, neutral $AlPO_4$ entities would probably interact more readily with the nonprotonated MA, and eventually yield a crystalline $AlPO_4$ (in this case IST-2). In other words, TEA prevents the cocrystallization of various $Al_xP_yO_z$ type amorphous phases with CoIST-2, by keeping them in solution through complexation. The presence of Co(II) ions in the synthesis batch does not seem to influence the sole role of MA as template for IST-2, as ascertained by the absence of ^{13}C NMR resonances typical of TEA^+ ions.

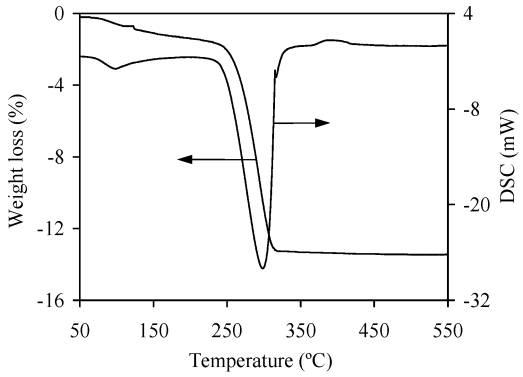

Figure 3. TG-DSC diagrams of CoIST-2.

Surprisingly, the Kjeldahl determination of N-bearing compounds evolved during the sharp weight loss indicates that both water and MA were released during this decomposition step. This confirms that, as in AlPO-53(A),[21] the presence of both moieties is important in the enhancement of the template and helps to strongly stabilize the final structure.

The ^{13}C NMR spectrum of CoIST-2[24] shows a single resonance at 27.39 ppm, similar to the one at 27.30 ppm recorded for IST-2.[21,24] Recent ab initio calculations have shown that such a shift is characteristic of nonprotonated methylamine molecules incorporated in various $AlPO_4$ pore structures.[25] This suggests that, as in the case of IST-2, MA is nonprotonated, despite the generation of negative charges in the framework induced by Co(II) incorporation. We can assume that the framework charges are counterbalanced by protons generated either by thermal degradation of the template or, alternatively, as suspected for IST-2,[21] that they originate from a slight excess of phosphoric acid used during the synthesis. The presence of such protons was clearly evidenced by FTIR (see below).

By comparison to JDF-2[17] and its analogue GaPO-AEN,[16] that both involve only protonated MA entities which solely counterbalance the negative charges of an equivalent number of OH^- groups linking two neighboring AlO_4 (GaO_4) groups in the structure, our NMR data[21] strongly suggest that we are dealing with neutral MA structural entities in both IST-2 and CoIST-2. Among the other isotypic $AlPO_4$ type compounds, only MCS-1[15] and AlPO-53(A)[18] also appear to contain neutral MA in their structures. The structure of MCS-1 was resolved in the calcined phase and the position of MA in the corresponding as-synthesized compound was not investigated. In the AlPO-53(A) structure, although the position of "dumbbell shaped" methylamine species and neighboring water molecules was not accurately documented, based on atomic distances calculated from atomic coordinates, it appears that both MA and water molecules are weakly bonded to the framework oxygens. The structure of IST-2 was shown to be very similar to that of AlPO-

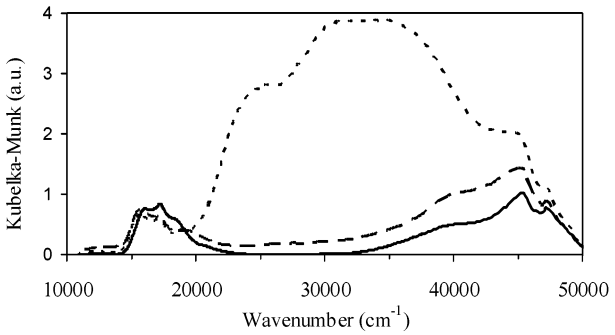

Figure 4. Diffuse reflectance UV−vis spectra of as-synthesized (solid line), calcined (doted line), and reduced (dashed line) CoIST-2.

53(A), so it is reasonable to assume that the positions of water and MA in its voids are also similar. In AlPO-53(A), the nitrogen atoms are at hydrogen bonding distances from framework oxygens, with no coordination to Al atoms, as are the two water molecules in the structure.[18] These features confirm that both (neutral) water and MA are also playing complementary templating and pore filling roles in IST-2 and in its cobalt analogue.

On the basis of the above chemical and thermoanalytical data, the unit cell composition was therefore concluded to be as follows: CoIST-2, $[Al_{23.2}P_{24.0}Co_{0.8}O_{96}]$ 8.0MA·13.5H_2O, and IST-2, $[Al_{24}P_{24}O_{96}]$ 7.7MA·15H_2O,[21] to be compared with AlPO-53(A), $[Al_{24}P_{24}O_{96}]$ 8MA·14H_2O.[18]

(2) Spectroscopic Evidence for the Presence of Framework Co(II) Ions. *Diffuse Reflectance UV−vis Spectroscopy.* Figure 4 shows the DR UV−vis spectra of as-synthesized CoIST-2 and the same material treated under oxidative and reductive conditions. The as-synthesized CoIST-2 material exhibits the characteristic absorption bands of the $^4A_2(F) \rightarrow {}^4T_1(P)$ transition (split by a dynamic Jahn−Teller effect or spin−orbit coupling) that occurs for divalent cobalt ions in tetrahedral coordination (i.e., bands with maxima at 10 600, 17 300, and 18 450 cm^{-1}). It is thus well-accepted and documented that these bands confirm the insertion of Co(II) into tetrahedral framework positions in $AlPO_4$ type materials.[5,8,27]

The spectrum of calcined CoIST-2 is dominated by strong and broad absorption bands in the range 20000−40000 cm^{-1}, with maxima at ca. 25000 and 32000 cm^{-1}. These new bands, coupled with the significant decrease in intensity of the absorption in the range 15000−20000 cm^{-1}, contribute to the well-known color change from blue to yellow-green observed after calcination of CoAPOs.[10,28,29] The intensity of the absorption corresponding to the tetrahedrally coordinated cobalt decreases by about 30%, thus indicating that the same proportion of Co(II) species readily change their coordination and/or oxidation state upon oxidative calcination. The larger splitting of the triplet is attributable to the presence of more distorted tetrahedral CoO_4 units in the calcined sample than in its as-synthesized counterpart. The broad and intense absorption at 20000−40000 cm^{-1} is currently assigned to charge-transfer bands associated with the formation of trivalent framework cobalt species[5,28,30] but also to distortion-induced charge-transfer effects without changing the oxidation state of the cobalt centers.[6,10,31] The formation of dispersed extraframework Co_xO_y species during the calcination procedure cannot be excluded[10] and, if so, it is also reasonable to attribute (part of) this broad absorption to charge-transfer bands associated with nonframework Co(III) species.

The reductive treatment carried out on calcined CoIST-2 significantly reduces the intensity of the high-frequency absorption bands, suggesting that most of the Co(II) and/or Co(III) framework species recover their initial structural state upon reduction, thereby confirming their framework positions. However, these bands associated with framework tetrahedral cobalt do not recover their initial intensity, confirming that during the thermal treatments more than one form of cobalt is generated and that a small part of such species was possibly extracted from their framework positions during the treatment. We can conclude so far that while the reversible oxidation of most of the framework Co(II) to Co(III) is probably responsible for the spectral changes that occur after calcination and further reduction (Figure 4), these results also indicate that a small but significant part of the framework cobalt suffers irreversible modifications (i.e., irreversible oxidation and formation of extraframework cobalt species).

Electron Paramagnetic Resonance Spectroscopy. The nonnormalized EPR spectra of the as-synthesized and calcined CoIST-2 sample are shown in Figure 5, parts a and b, respectively. The X-band EPR spectrum of the fresh material produced a poorly resolved signal over a large field range (from ∼500 to ∼6000 G; 10 G = 1 mT). At least three components appear to be visible in this spectrum with approximate g values of 5.94, 2.33, and 1.64. The component at $g = 5.94$ appears to be structured with a number of poorly resolved (possibly) hyperfine lines. However, the spectrum is insufficiently resolved to unambiguously confirm that these lines arise from ^{59}Co hyperfine interactions (where $I = {}^7/_2$ for ^{59}Co). A very weak symmetrical signal is also evident at $g = 2.0023$, which most likely arises from traces of radical impurities, and will not be discussed further. After calcination, the EPR spectrum changes dramatically (Figure 5b). First, the spectrum becomes simpler and reduces to two principal components characterized by g values of ∼5.94 and ∼2.2. Again traces of a minor signal can also be seen at free spin. Second, the intensity of the EPR signal appears to decrease (ca. 20−30%) upon calcination, suggesting an apparent decrease in the number of paramagnetic cobalt species. No ENDOR spectra (Electron Nuclear DOuble Resonance) could be observed from either the as-synthesized or calcined samples (due to the broad EPR line widths, and therefore a weak ENDOR response, and also due to the unfavorable relaxation times). Variable-temperature EPR experiments were also carried out on the as-synthesized and calcined samples between 10 and 30 K. In both cases the intensity of the EPR signal decreased dramatically as the temperature was raised to 30 K.

EPR has been used in the past to characterize the nature of cobalt-containing aluminophosphates.[6,27,32,33] In many of these papers, particular attention was devoted to the cause of the changes in EPR signal intensity in the as-synthesized versus the calcined samples. While there was some initial evidence in the literature that the change (i.e., reduction) in EPR signal intensity in the fresh and calcined samples was due to changes in the oxidation state of cobalt (i.e., from EPR active Co(II) to EPR silent Co(III)),[34] this observation was later challenged and has now been unambiguously explained on the grounds of changes in distortions to the framework Co(II) ions. Weckhuysen et al.[32] clearly demonstrated that most of the Co(II) in cobalt-containing aluminophosphates (AlPO-5, -11, -44, and -46) is in fact EPR active with only about 30% of this cobalt undergoing oxidation to Co(III) after calcination. In the present case of CoIST-2, a similar intensity change was noted after calcination, thereby suggesting that about 25% to 30% of framework Co(II) was oxidized to (framework and/or nonframework) Co(III).

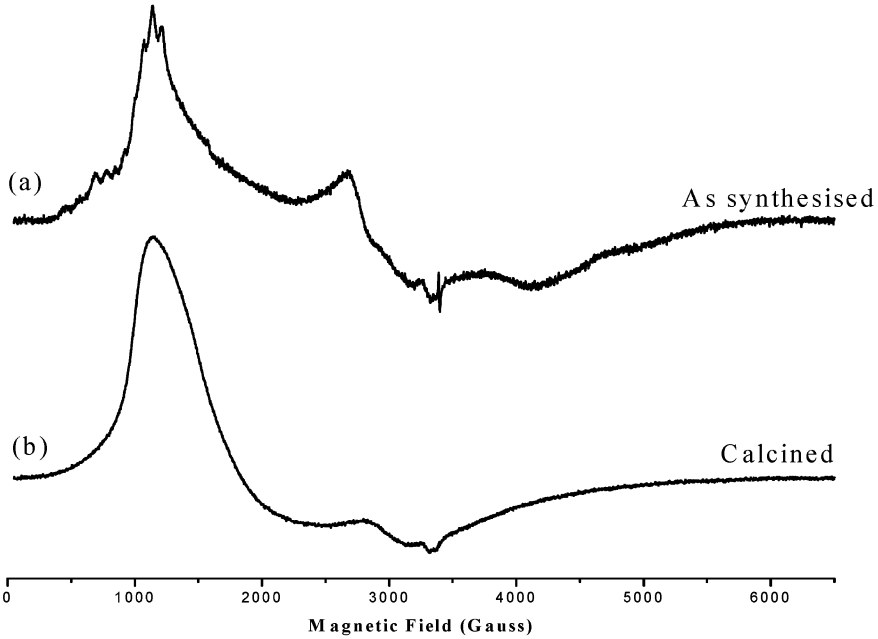

Figure 5. CW EPR spectra (X-band) of CoIST-2 recorded at 10 K: (a) as-synthesized and (b) calcined sample.

When cobalt(II) exists in a purely tetrahedral environment, it has the orbital singlet Γ_2 lowest in energy. Since $S = {}^3/_2$, there is a 4-fold spin degeneracy. In practice, the sites are always distorted, whereby the 4-fold spin degeneracy is partly removed, leaving two closely spaced Kramers doublets ($m_s = \pm{}^1/_2$ and $m_s = \pm{}^3/_2$), which are degenerate in the absence of an applied magnetic field. The splitting between the two doublets is known as the zero field splitting (Δ), which is characterized in the EPR spectrum by the zero field splitting parameters D and E. When Δ is larger than the microwave energy ($\Delta \gg h\nu$), such transitions as observed in EPR are those that occur within each of the two Kramers doublets. The sign of Δ is determined by whether the $m_s = \pm{}^1/_2$ or $m_s = \pm{}^3/_2$ doublet lies lowest. When $m_s = \pm{}^1/_2$ is lowest, the sign of Δ is positive and when $m_s = \pm{}^3/_2$ is lowest, the sign of Δ is negative. This has important implications on the temperature dependency of the EPR transition. When the zero field splitting is greater than 0 cm^{-1} (i.e., positive Δ), a Curie−Weiss behavior will be observed, whereas a non-Curie−Weiss behavior is predicted in the opposite case, involving a negative Δ. From the EPR measurements recorded between 10 and 30 K for CoIST-2, the signal intensities decreased significantly as expected for a Curie−Weiss behavior. This suggests that the value of Δ for Co(II) in CoIST-2 is positive and the $m_s = \pm{}^1/_2$ doublet is lowest in energy, analogous to that reported[32] for framework-incorporated Co(II) in a distorted tetrahedral site.

Banci et al.[35] published a review which shows that the g factors themselves do not unequivocally distinguish between the different coordination states of the Co(II) ion (i.e., 4-, 5-, and 6-coordinate). High-spin cobalt(II) ions in 6- and 5-coordinate environments usually show hyperfine structure (while tetrahedral cobalt(II) does not), and while this was heralded initially as evidence for particular changes in geometry,[36] this is not easy to prove, and represents a very "risky" approach to assign a signal particularly in a polycrystalline microporous material where line broadening is expected. An alternative approach was discussed by Makinen et al.[37] based on the magnitude of the zero field splittings, which apparently follow the trend $\Delta_4 < \Delta_5 < \Delta_6$ (i.e., the separation between the two Kramers doublets are smallest for a 4-coordinate Co(II) ion and largest for a 6-coordinate ion). The magnitude of the zero field splitting can be determined by using the microwave saturation technique,[32,37] which is based on the relationship between the saturating microwave power ($P_{1/2}$) and both the spin−lattice (T_1) and spin−spin (T_2) relaxation times (where $P_{1/2} \propto 1/T_1 + 1/T_2$). Unfortunately, the cobalt content in our CoIST-2 sample was too large ($Al_{23.2}P_{24}Co_{0.8}O_{96}$) for this analysis, since $1/T_2$ will be significantly perturbed in this case with the large Co(II) concentration, and therefore a reliable and confident extraction of Δ from the data is not possible. However, this analysis was carried out by Weckhuysen et al.,[32] and they unequivocally demonstrated that $\Delta = 7$ cm^{-1} (i.e., 4-coordinate Co(II)) for their Co(II)-containing aluminophosphate. Using that value, they successfully simulated the EPR spectrum.

The EPR spectrum of the calcined sample in Figure 5b is characterized by a broad, axially symmetric signal with effective g values of $g_\perp \approx 5.80-5.44$ and $g_{||} \approx 2.05$. These g values are similar to those previously reported for CoAPO-5 and CoAPO-41 and we used g, D, and E values, typical of tetrahedral Co(II) in a distorted symmetry, to simulate the experimental spectrum. The parameters used were $g_x = 2.44$, $g_y = 2.44$, $g_z = 2.02$, $D = 3.5$ cm^{-1}, and $E = 0$ cm^{-1} (where $\Delta = 2(D^2 + 3E^2)^{1/2}$). A reasonable fit between the experimental and simulated spectrum was obtained, particularly with respect to the peak positions. Due to limitations in the program used, we were unable to satisfactorily simulate the EPR line shape accurately. Nevertheless it can be stated that the spectrum shown in Figure 5b can be confidently assigned to Co(II) in a distorted tetrahedral environment, with a temperature-dependent profile that reveals a Curie−Weiss behavior indicating an $m_s = \pm{}^1/_2$ ground state of the high-spin Co(II) ion and the zero field splitting $\Delta > 0$ cm^{-1}.

A final comment should be made with respect to the spectrum of the fresh as-synthesized material (Figure 5a). The spectrum appears to have a rhombic profile with g values of 5.94, 2.33, and 1.64. In previous EPR studies of Co containing aluminophosphates, the spectra of the as-synthesized and calcined samples were similar (apart from the changes to the signal intensity).[8,27,32,33] The spectrum in Figure 5a can best be interpreted as a composite signal arising from a contribution of two high-spin cobalt(II) ions, both in slightly different distorted

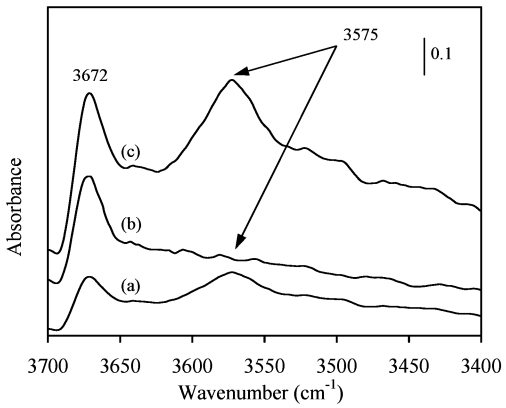

Figure 6. FTIR spectra of CoIST-2: (a) as-synthesized, (b) calcined, and (c) reduced.

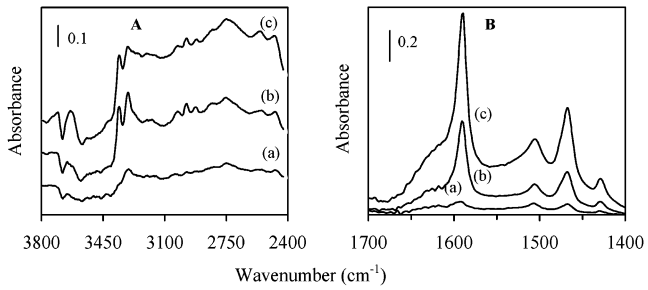

Figure 7. Difference FTIR spectra of methylamine adsorbed on reduced CoIST-2 under increasing methylamine pressures of (a) 0.3, (b) 1, and (c) 3 Torr, recorded in (A) the 3800−2400 and (B) 1700−1400 cm^{-1} range.

tetrahedral environments. One species is axially symmetric (flattened or elongated tetrahedron − D_{2d}) with g values of ∼5.94 and ∼2.2 (as discussed above) while the other is rhombic (5.94, 2.33, and 1.64). These latter values are not dissimilar to those observed for cobalt pyridine chloride with $g = 1.77$, 2.62, and 5.82 (hyperfine structure not resolved) where the cobalt also exists in distorted tetrahedral sites.[36] Clearly in the small-pore IST-2 structure, interaction occurs between the framework Co(II) ions and surrounding template molecules in this fresh as-synthesized material, creating subtle differences in the EPR spectra, not commonly observed in wide-pore materials.

(3) FTIR Evaluation of Acidity. *FTIR Investigation of Hydroxyl Groups.* The isomorphous substitution of Co(II) for Al(III) in the tetrahedral framework of IST-2 should generate a negatively charged lattice. Usually, in this class of materials, the negative charges are compensated by the positive template ions that, upon calcination, leave a proton and give rise to the formation of Brönsted type acid sites which can subsequently be studied by FTIR.

Figure 6 shows the FTIR spectra of CoIST-2 in the range 3400−3700 cm^{-1} obtained after different treatments. The spectrum obtained after evacuation at 120 °C (with methylamine still inside the porous structure) shows bands with maxima at 3672 cm^{-1} (assigned to P−OH and Al−OH terminal groups) and 3575 cm^{-1} (attributed to Co(OH)P groups[7,38]). The existence of the band at 3575 cm^{-1} with MA still present indicates that the framework negative charges are compensated by protons and not by the template, since ^{13}C NMR confirmed that MA was not protonated. Such protons could originate from traces of unreacted phosphoric acid.[21]

The band associated with Co(OH)P completely vanishes upon oxidative calcination of the sample and is restored after a reductive treatment. This observation confirms the hypothesis of a reversible oxidation of at least part of the framework cobalt. It should be noted that part of the divalent tetrahedrally coordinated cobalt changes neither its coordination nor its oxidation state upon calcination, as suggested by EPR and UV−vis spectroscopy and confirmed by electrochemical data (see below). Moreover, while P−OH and/or Al−OH groups are still present in the calcined compound (i.e. residual band at 3672 cm^{-1}), the protons responsible for the Brönsted acidity—Co(OH)P—have disappeared. This explains why, in the absence of bridging OH groups, the framework tetrahedral Co(II) ions become distorted (UV−vis).

The formation of a framework oxygen vacancy in the vicinity of the incorporated Co(II) ions has been envisaged to explain the resistance of such Co(II) species to oxidation.[9,38] On the other hand, Sponer et al.[10] suggested, for as-synthesized CoAPO-11, a template−framework interaction between electron donor and acceptor pairs where a Co−O bond is replaced by a Co−N bond. Assuming this model is valid for part of the incorporated Co(II) ions, then the removal of the template could be responsible for the generation of the oxygen vacancies. In our case, the fact that the N-bearing template (MA) is only weakly bonded to the framework[25,26] does not argue in favor of this hypothesis. Therefore, for CoIST-2, an alternative explanation for the thermal generation of oxygen vacancies should be proposed based on a process similar to the dehydroxylation of aluminosilicates during calcination.[39]

Finally, the oxygen vacancy model only accounts for the improved stabilization of Co(II) in the framework but does not exclude the possibility that, even if it is oxidized to Co(III), it can stay positioned in its original framework sites and thereby readily undergo a reversible reduction. Framework structural constraints can also be considered to explain the stability of the framework Co(II) species and, thereby, their ease of oxidation, followed by their extraction from the framework (see below).

Methylamine Adsorption. Adsorption of methylamine on calcined CoIST-2 was performed to complement the characterization of the acidic properties of this material. This probe molecule was selected due to its small size and basic characteristics. The FTIR spectrum of gaseous methylamine displays the asymmetric and symmetric stretching vibrations of N−H bonds respectively at 3427 and 3361 cm^{-1}, the asymmetric bending vibration of H−N−H at 1623 cm^{-1}, the stretching vibrations of C−H at 2985, 2961, and 2820 cm^{-1}, and a group of bands relative to the bending vibration of H−C−H at 1485, 1473, and 1430 cm^{-1}.[40]

After the first admission of methylamine onto reduced CoIST-2 (0.3 Torr), the FTIR spectrum (Figure 7a) shows a small decrease of the band at 3672 cm^{-1} and of the band assigned to Co(OH)P Brönsted acid sites (3575 cm^{-1}). Additionally a set of small and broad bands located at 2748, 2553, and 2475 cm^{-1} is already visible. The bands in this spectral range can be assigned to the asymmetric and symmetric N−H stretching vibration of the $CH_3NH_3^+$ ion resulting from the interaction of methylamine with the negative charge located close to the framework Co(II) species (assuming that methylammonium cations progressively replace protons of the Co(OH)P species). The bands recorded at 3354, 3305 (Figure 7A), and 1590 cm^{-1} (Figure 7B) can be respectively assigned to the asymmetric and symmetric stretching vibration of N−H bonds and asymmetric bending of H−N−H of methylamine adsorbed on Lewis acid sites.[41] Bands located at 1505, 1466, and 1429 cm^{-1} are due to the H−C−H bending vibration of the adsorbed methylamine.

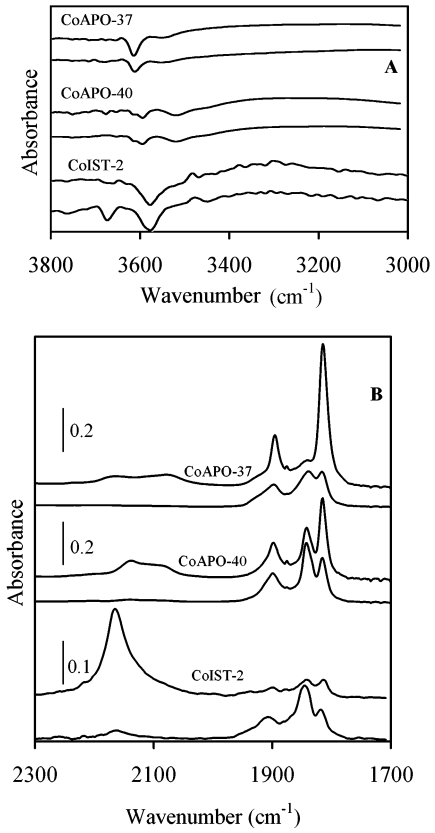

Figure 8. Difference FTIR spectra of reduced CoIST-2, CoAPO-40, and CoAPO-37 after adsorption of 0.5 (lower traces) and 13 Torr (upper traces) of NO in (A) the 3800−3000 and (B) the 2300−1700 cm^{-1} range.

The increase in the amount of methylamine adsorbed is coincident with the parallel decrease in the intensity of the band assigned to Co(OH)P species, thereby confirming that the protons in such sites are progressively replaced by $CH_3NH_3^+$ ions. However, the bands assigned to vibrations of methylamine adsorbed on Lewis acid sites also increase with loading, showing that a large number of these acid sites are also present in the sample, possibly generated upon the successive oxidation and reduction treatments at elevated temperature.

(4) Investigation of Differently Structured Cobalt Species by FTIR of Adsorbed NO. Figure 8 displays the FTIR spectra of three cobalt-containing aluminophosphates, CoIST-2, CoAPO-40, and CoAPO-37 (precalcined in air and then reduced with H_2), after adsorption of 0.5 and 13 Torr of NO. This figure is divided in two parts: the first part corresponds to the region of the vibration of hydroxyl bands (3800−3000 cm^{-1}) and the second part corresponds to the nitrosyls region (2300−1700 cm^{-1}). The interaction of NO with the protons of the Co(OH)P groups is clearly seen by the decrease of the band at 3575 cm^{-1} for both NO loadings with respect to the reference spectra (negative absorbance) and by the parallel increase of a broad band with maximum at ca. 3300 cm^{-1}. As expected, a higher pressure of NO is required to observe its interaction with terminal P−OH and Al−OH groups (3672 cm^{-1} band).

Upon the first admission of NO, the spectrum shows a set of bands in the 1750−1950 cm^{-1} range along with a low-intensity band at 2160 cm^{-1}. The decomposition of the spectrum shown in Figure 8B for CoIST-2 (0.5 Torr NO), in the range 1750−2000 cm^{-1}, yields six bands with maxima at 1813, 1840, 1865, 1899, 1907, and 1937 cm^{-1} (see Supporting Information). The low-intensity band at 1937 cm^{-1} has been assigned by Hadjiivanov et al.[42] to linear Co(III)−NO species. Most of these Co(III) ions are generated during the first oxidative calcination process although we cannot exclude the possibility that partial reoxidation of some Co(II) ions occurs by adsorbed NO. As confirmed by UV−vis data, the reductive treatment that follows the precalcination in air does not lead to a reversible reduction of all the Co(III) species. Some remain in the (III) oxidation state (Co_xO_y type species), suggesting that they are probably no longer in lattice positions and that their formation is definitely irreversible.

It is generally accepted that when NO is adsorbed onto Co(II) ions, it forms mainly dimeric compounds which are characterized by symmetric stretching vibrations in the range 1910−1875 cm^{-1} and asymmetric stretching vibrations in the range 1830−1785 cm^{-1}.[42−45] Taking these data into account and based on similar results found by Gianotti and co-workers[44] for CoAPO-18, it is possible to identify the presence of two different nitrosyl complexes formed by adsorption of NO on Co(II), characterized by a set of bands at 1840 and 1907 cm^{-1} and another at 1813 and 1899 cm^{-1}. The formation of two different complexes upon NO adsorption can be justified by the existence of two structurally different Co(II) ions that were also detected by UV−vis and cyclic voltammetric measurements on the air-calcined and reduced samples (see below).

So far, in the oxidized sample, FTIR data have shown that most of the Co(OH)P Brönsted acid sites have disappeared (Figure 6b) and that most of them were restored after further reduction (Figure 6c). When NO is adsorbed onto the oxidized sample, all the bands in the range 1750−1950 are present in the spectrum (see Supporting Information). Nevertheless, the relative intensity of the doublet at 1840 and 1907 cm^{-1} is lower than that in the FTIR spectrum corresponding to the reduced sample (see Supporting Information). This fact strongly indicates that the doublet at 1840−1907 cm^{-1} can be assigned to the nitrosyl complex formed on Brönsted Co(OH)P sites. Although these bands seem to have completely vanished from the FTIR spectra (Figure 6b), the presence of the NO dinitrosyl complex (more sensitive IR bands) indicates that a small amount of such sites remains even after calcination. So, the second set of bands (1813−1899 cm^{-1}) correspond to dinitrosyl complexes involving Co(II) species that are not of the Brönsted type, but rather correspond to Lewis centers such as those detected upon methylamine adsorption. Indeed, Marchese et al.[29] have attributed similar IR bands to such species.

The above set of results allowed us to conclude that at least two types of Co(II) species can be detected and their evolution under different redox treatments may be summarized as follows:

air-calcination	H_2-reduction
Co(II) as Brönsted Co(OH)P Species	intensity increases
Co(II) as Lewis Co□P species	intensity slightly increases

The assignment of the bands in the range 2100−2400 cm^{-1} on various zeolite (porous) and non-zeolite (bulk) systems is still controversial. NO^+, NO_2^+, and $NO_2^{\delta+}$ species have been suggested to be responsible for the presence of a band usually seen at 2133 cm^{-1} for zeolite-type materials.[42,44−47] The mechanism currently proposed for the formation of such species in zeolites involves Brönsted acid sites and/or the presence of molecular oxygen. Nevertheless, bands in that region which have been assigned to the same species were also observed after NO adsorption on fully metal-exchanged Co-ZSM-5.[43]

In our case, the band at 2160 cm^{-1} (Figure 8B) does not result from species that were formed mainly by a mechanism involving the Brönsted acid sites. Indeed, as described above, upon the

TABLE 2: Structural Properties of AEN, AFR, and FAU Topologies

topology	channel system[a]	framework density
AEN B[b] (CoIST-2)	[100] **8** 3.1 × 4.3* ↔ [010] **8** 2.7 × 5.0*	19.7
AFR (CoAPO-40)	[001] **12** 6.7 × 6.9* ↔ [010] **8** 3.7 × 3.7*	15.0
FAU (CoAPO-37)	⟨111⟩ **12** 7.4 × 7.4***	12.7

[a] International abbreviations as in ref 20. [b] Structure data of AlPO-53 (B), which corresponds to our calcined and/or reduced CoIST-2.

first admission of NO, the bands corresponding to the Brönsted OH groups (3575 cm^{-1}) almost completely vanished and, at that stage, the band at 2160 cm^{-1} shows a low intensity (Figure 8B). The increase of NO pressure to 13 Torr leads to a significant increase of this band and to a decrease of the band corresponding to terminal OH groups (3672 cm^{-1} peak in Figure 8A) while there is no significant intensity change in the band assigned to Brönsted acid sites (3575 cm^{-1}). In addition, this band (2160 cm^{-1}) has a high intensity at low NO dosage on the oxidized sample (see Supporting Information) that contains only a small amount of Brönsted acid sites as stated before.

We therefore propose that the adsorbed species that gives rise to the band at 2160 cm^{-1} may correspond to NO^+. The formation of this species can occur by the formal reduction of framework Co(III) ions that were generated through the oxidation of Brönsted Co(OH)P acid sites present in the as-synthesized phase during the calcination under O_2. The NO^+ formed could adsorb on a basic oxygen atom located near the Co(II) ion and thereby compensate the framework charge. This model would explain the increase of the band at 2160 cm^{-1} on an oxidized sample and also the fact that the reduction of Co(III) does not give rise to the increase of the bands associated to OH groups belonging to Co(OH)P. Increasing the NO pressure in the IR cell also generally leads to the formation of surface nitro-nitrate species characterized by new bands arising below 1700 cm^{-1}.[43]

The results reported here for CoIST-2 confirm our UV−vis and FTIR findings, namely that part of framework Co(II) is oxidized to Co(III) before the generation of NO^+ species stemming from (adsorbed) NO. This is in agreement with similar findings by Gianotti and co-workers[44] for CoAPO-18. These authors additionally reported the formation of N_2O, which could be associated with the oxidation of Co(II).

The adsorption of NO was also performed on CoAPO-37 (with composition $(Co_{0.02}Al_{0.48}P_{0.50})O_2$[48]) and CoAPO-40 (with composition $(Co_{0.01}Al_{0.49}P_{0.50})O_2$[7]) to investigate the influence of the framework (pore) structure on the adsorption of NO. CoAPO-37 has a Faujasite type structure (FAU) involving supercages (with 12-membered-ring openings) and sodalite cages, while the channel structure of CoAPO-40 (AFR type) involves 12- and 8-membered-ring intersecting channels and some side pockets.[20,49] Table 2 summarizes the structural features of the three materials investigated. Figure 8 also shows the FTIR spectra of adsorbed NO (0.5 and 13 Torr) on samples of CoAPO-37 and CoAPO-40 that were calcined in air and further reduced. Similar to CoIST-2, a set of bands in the range 1750−1950 cm^{-1} is present in all spectra. As discussed above, we assign these bands to the formation of dinitrosyl groups on Co(II). The bands assigned to hydroxyl groups almost completely vanish upon the first admission of NO (0.5 Torr; Figure 8A) while, in contrast to CoIST-2, no band of significant intensity was observed in the region 2000−2300 cm^{-1}.

When the NO pressure is increased to 13 Torr, at least two weak and broad bands appear in that region (2100 and 2140 cm^{-1} for CoAPO-40 and 2080 and 2170 cm^{-1} for CoAPO-37). A different behavior from that of CoIST-2 has also been observed regarding the bands in the dinitrosyl region: a small decrease of the intensity of the bands at 1840 and 1920 cm^{-1} and the parallel increase of the bands at 1814 and 1900 cm^{-1} suggests that the decrease of the initial amount of Co(II) (probably as a result of oxidation to Co(III) that was present before NO adsorption) is smaller than that observed for CoIST-2. Assuming, as discussed above, that the formation of the species that gives bands in the 2000−2300 cm^{-1} region (probably NO^+) is enhanced by the reduction of Co(III), the decrease of the bands at 1840 and 1920 cm^{-1} suggests that these bands are associated with Co(II) centers that are able to change their oxidation state. Consequently, such species probably belong to Co(OH)P Brönsted acid sites, which confirms our previous assignment (NO adsorbed on CoIST-2).

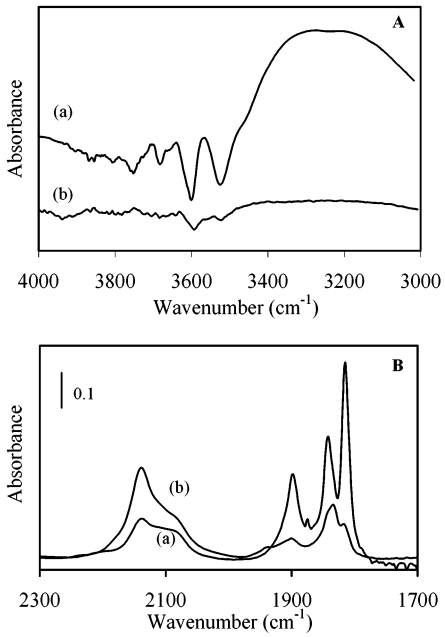

Figure 9. FTIR spectra of CoAPO-40 after adsorption of NO: (a) adsorption of 13 Torr of NO onto a reduced sample and (b) adsorption of 0.2 Torr of NO onto a calcined sample. The spectra were recorded in (A) the 4000−3000 and (B) 2300−1700 cm^{-1} range.

The occurrence of at least two bands in the range 2000−2300 cm^{-1} contrasts with our observations for CoIST-2 and could be related to different locations of the cobalt ions that interact with NO^+ in the porous structures of CoAPO-37 and CoAPO-40, i.e., in respectively large (supercage) and small (sodalite cages) cavities in the FAU structure and in channels and side-pockets in the AFR structure.

The overall behavior of air-calcined CoAPO-40 is similar to that of calcined CoIST-2. It is clear from the spectrum shown in Figure 9 that the presence of Co(III) cannot be dissociated from the formation of the species that absorb in the range 2000−2300 cm^{-1}. Indeed, the intensity of the bands in this range is higher upon adsorption of 0.2 Torr of NO than the intensity of the same bands upon adsorption of 13 Torr of NO on a reduced sample (which should contain fewer Co(III) ions). The comparison of the behavior of CoIST-2, CoAPO-37, and CoAPO-40 upon NO adsorption suggests that the framework Co(II) in CoAPO-37 and CoAPO-40 is more resistant to the oxidation than it is in CoIST-2. Figure 8 shows a much higher decrease of the bands assigned to dinitrosyls on Co(II) in reduced CoIST-2 than on the other two structures, when the pressure of NO increases. A similar behavior was already reported for

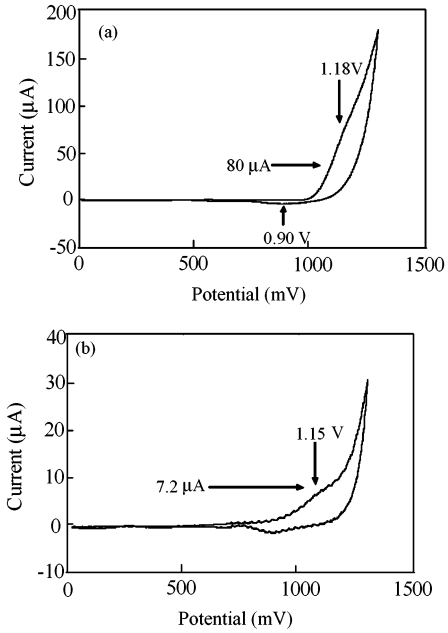

Figure 10. Cyclic voltammogram of (a) as-synthesized and (b) calcined CoIST-2.

CoAPO-18 (framework density of 14.8) when compared with CoAPO-5 (framework density of 17.3).[44]

The resistance to the oxidation of framework Co(II) seems to be highly dependent on the porous structure as reported by Verberckmoes et al.[27] and Barrett et al.[30] and is probably related to the constraints that exist in the more dense structures, which lead to local distortions. These distortions are responsible for a less steady stabilization of the framework Co(II) ions and thus to its ease of oxidation. A strained framework would indeed involve local distortions that would more readily destabilize the lattice Co(II) ions and thereby lead to their easier oxidation under appropriate conditions. In other words, the degree of distortion of the cobalt site and, hence, its ease to undergo oxidation are dependent on the framework type and, more specifically, on the structure density. A separate study of this effect in the three CoAPO samples by cyclic voltammetry is reported elsewhere,[50] and demonstrates the additional importance of solvent screening effects on the redox properties of the cobalt ion.

(5) Electrochemical Evaluation of Redox Properties of CoIST-2. *Electrochemical Oxidation of As-Synthesized CoIST-2.* The redox behavior of the cobalt species present in the as-synthesized samples was also investigated by cyclic voltammetry (CV), a technique that proved useful in the case of other metal-bearing porous solids.[50−52] Figure 10a shows the cyclic voltammogram of as-synthesized CoIST-2 embedded in a carbon paste modified electrode, in the 0−1.3 V range. While MA template is still present in the as-synthesized material, and should undergo electrochemical oxidation, the oxidation peak observed at ca. 1.18 V can be confidently assigned to an oxidation of Co(II) to Co(III). This assignment was based on a "blank" experiment, in which the CV of a cobalt-free IST-2 sample (containing MA) was recorded and did not show the dominant peak at 1.18 V (only a small unresolved peak at ca. 0.5 V with a residual current density of less than 10 μA, was observed). Furthermore, the peak assigned to Co oxidation is also observed in the template-free, calcined sample (Figure 10b).

At this stage, it is not possible to discriminate between the various structural configurations of these electrochemically generated Co(III) species (i.e., framework vs nonframework). Nevertheless, the wave type peak shape is characteristic of an electronic transfer associated with a chemical reaction originating from the extraction of the oxidized Co species from its framework position.

On the reverse scan (cathodic range), the voltammogram exhibits an ill-defined, weak and broad peak (at ca. 0.90 V, as indicated by the arrow in Figure 10a). Assuming this weak peak is significant, it can be logically attributed to the reversible reduction of the framework Co(III) species, as is also seen by UV−vis and not contradicted by FTIR. The fact that its overall intensity is weak indicates that a relatively large part of the Co(III) ions do not reintegrate their framework positions, at least after electrochemical oxidation. This confirms the "chemical reaction" suggested by the shape of the oxidation peak, namely the removal of Co(III) from the framework and the further possible migration of such Co_xO_y particles either toward the external surface of the sieve material or into their channel system. As the significance of this peak is still questionable, its possible absence could also reflect the dramatic difference in the electrochemical oxidation and/or reversible reduction processes that, opposite to the high-temperature oxidations, basically occur without any chemical reducing species and at ambient temperature (in stark contrast to the high-temperature oxidations). It should be clearly stated therefore that the nature and abundance of the oxidized cobalt species generated in the electrochemical experiment may be different compared to the distribution of cobalt species generated under oxidized (in air flow) or reduced (under H_2 flow) conditions at 400 °C.

Electrochemical Oxidation and Reduction of Air-Precalcined CoIST-2. To evaluate semiqualitatively the relative amount of Co(II) and Co(III) species generated during the air calcinations at 400 °C, the air-calcined CoIST-2 was also oxidized and further reduced electrochemically under the same conditions as described above for the as-synthesized material.

First, comparison of the electrochemical oxidation of the as-synthesized (Figure 10a) and air-calcined CoIST-2 samples (Figure 10b) reveals the presence of an anodic peak corresponding to Co(II) → Co(III) oxidation at about the same potential, namely +1.15 V, but the current was very different. A semiqualitative evaluation of the current intensity recorded in both cases (80 μA for the as-synthesized CoIST-2 and 7.2 μA for the calcined phase) resulted in a decrease of about 90% of this current for calcined CoIST-2. The first conclusion is that only about 10% of Co(II) was left in the sample and that the calcination resulted in the oxidation of about 90% of the initial framework Co(II), yielding Co(III) in two different structural states (see above UV−vis data). This result is, however, in dramatic contradiction with the results derived from EPR and UV−vis (where only an approximately 30% oxidation was observed). Even if the absolute and accurate evaluation of the UV−vis peak intensities is only approximate, it is clear that the difference between the 30% oxidation evaluated during air calcinations with respect to the 90% oxidation evaluated in the electrochemical experiment is significant.

To reconcile these discrepancies, one can assume that not all of the Co(II) species in the calcined phase were probed by cyclic voltammetry, possibly because, unlike the situation observed for the as-synthesized material, we are dealing with at least two structurally different Co(II) species. One such species escapes the electrochemical detection, possibly because of the limited anodic potential windows used. To confirm this hypothesis, oxidation of the CoIST-2 sample was again performed by using a less restrictive technique, namely "Square Wave Voltammetry" (SWV). Because the potential range is now swept more slowly, this technique can detect the same oxidation

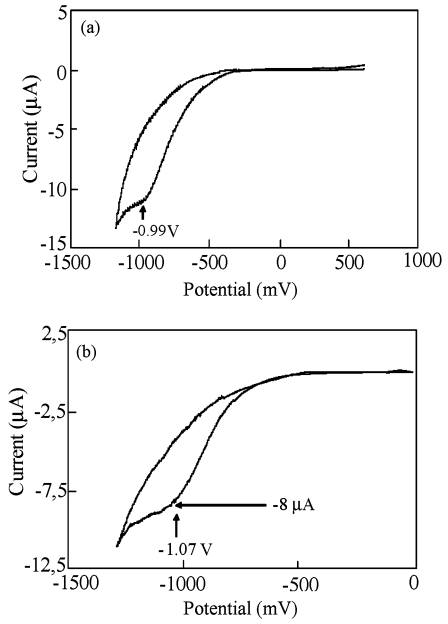

Figure 11. Cyclic voltammogram of a cathodic reduction of (a) as-synthesized and (b) calcined CoIST-2.

and reduction phenomena that would now occur at less negative potentials (by about 0.15 V). In the SWV voltammogram, one could indeed detect the "missing" or unaccounted for oxidation processes, not seen previously by cyclic voltammetry, at about 1.0 V (figure not shown). This clearly demonstrates that most of the Co(II) ions have a different structural state and that their oxidation, occurring above 1.2 V under cyclic voltammetry conditions, was missed in the cyclic voltammogram. As any quantitative computation of such species should be inaccurate in SWV, we can conclude that the first semiquantitative evaluation of the total Co(II) species in the air-calcined phase by UV−vis (about 30% Co oxidized thus about 70% Co(II) left) may not be incorrect (within the limits of the evaluation of the band intensities in the UV−vis technique).

The cyclic voltammetry, combined with SWV, allowed us to detect at least two differently coordinated Co(II) species that coexist, along with the different Co(III) species, in the calcined phase. The existence of two such differently structured Co(II) species could also be undoubtedly confirmed by FTIR of adsorbed NO (see above).

The same samples were then cathodically reduced. Upon electrochemical reduction at a highly negative potential, all the framework Co(II) species in the as-synthesized and calcined material were readily and totally reduced at about the same potential to metallic cobalt particles, more precisely at −0.99 (Figure 11a) and −1.07 V (Figure 11b), respectively. It must be noted that this scheme is typical of the voltammetric experiments and that such particles are never obtained through any chemical reducing processes. As such reduction occurs at a similar potential for both phases with no extra peak detected for a Co(III) → Co(II) reduction in the calcined phase (Figure 11b), one can assume that this potential always corresponds to the transformation of total cobalt (Co(II) + Co(III)) to metallic cobalt.

Conclusions

A synthesis method has been described and optimized for the preparation of a pure and highly crystalline cobalt- substituted aluminophosphate, labeled CoIST-2, with an AEN type framework, similar to AlPO-53(A). The combination of the characterization techniques used in this work (UV−vis, EPR, FTIR, and cyclic voltammetry) collectively enabled us to (i) confirm, along with the unit cell expansion measured by XRD, that we are dealing with a true framework Co(II) insertion and (ii) to detect at least two differently structured Co(II) species incorporated in the crystalline framework. The precise synthesis steps required for the controlled and systematic variance of one site over the other are not known at the present. The UV−vis spectra of the fresh and calcined CoIST-2 material exhibited characteristic absorption bands of the $^4A_2(F) \rightarrow {}^4T_1(P)$ transition, typical of divalent cobalt in tetrahedral coordination. Most of the framework Co was found to be reversibly oxidized, with a smaller part undergoing irreversible oxidation during the calcination process. The EPR spectrum of the calcined sample was interpreted by using the spin Hamiltonian parameters of $g_x = 2.44$, $g_y = 2.44$, $g_z = 2.02$, $D = 3.5\ cm^{-1}$, and $E = 0\ cm^{-1}$, and assigned to cobalt(II) in a distorted tetrahedral environment (as expected for framework-incorporated Co(II)). The temperature-dependent profile (10−30 K) was found to be typical of a Curie−Weiss behavior with a positive zero field splitting. The EPR spectrum of the as-synthesized sample also indicated the presence of two different Co(II) environments, as characterized by different sets of g values. The electrochemical analysis of the redox behavior of CoIST-2 was also investigated. By using cyclic voltammetry (CV) and square wave voltammetry, the electrochemically induced oxidation of Co(II) → Co(III) in both the as-synthesized and air-calcined samples (partly oxidized) was confirmed, but owing to the different conditions employed in the electrochemical oxidation step, precise quantitative analysis of the redox process was not possible. Nevertheless CV provided clear evidence for the presence of at least two differently coordinated Co(II) species.

FTIR spectroscopy was used not only to evaluate the acidity of the surface hydroxyl groups but also, using NO as a probe molecule, to investigate the differently structured cobalt species. Two different types of framework cobalt species, differing in their behavior toward the nature of the acid site formed, and in their reversibility toward Co(II)/Co(III) redox behavior, were identified by FTIR of adsorbed NO. One of these cobalt species appeared to be responsible for the formation of Brönsted Co(OH)P acid sites while the other seemed to be associated with the presence of Lewis acid sites (Co□P type species). The FTIR data of adsorbed NO also demonstrated the relatively facile oxidation of Co(II) in the AEN structure of IST-2 compared to the more open FAU (CoAPO-37) and AFR (CoAPO-40) structures, highlighting the importance of framework density in the oxidative ability of framework cobalt ions in these structures. While the reversible oxidation of Co(II) to Co(III) is not excluded by the characterization techniques, the results reported here suggest that only the fraction of the Co(II) ions associated with the Brönsted acid sites participate in this process.

The results presented in this paper demonstrate the importance of utilizing a variety of characterization techniques for probing the heterogeneity of framework sites for heteroelements inserted into porous aluminophophate frameworks. More importantly, with respect to the general rationalization of the redox properties of such materials, the results have shown how redox properties of the metal ion are intimately linked to both the structure type/density and framework sitings of the transition metal ion.

Acknowledgment. The authors wish to warmly thank Dr. L. B. McCusker for pertinent comments regarding the IST-2 structure. M. R. Vataj is acknowledged for valuable technical help in electrochemical experiments. Prof. J. Rocha is gratefully

acknowledged for the NMR results. Financial support for this work by FCT, under the PRAXIS XXI program, is acknowledged.

Supporting Information Available: Deconvoluted FTIR spectrum of reduced CoIST-2 after adsorption of NO and dfference FTIR spectra of reduced and calcined CoIST-2 after adsorption of NO. This material is available free of charge via the Internet at http://pubs.acs.org.

References and Notes

(1) Vanoppen, D. L.; De Vos, D. E.; Genet, M. J.; Rouxhet, P. G.; Jacobs, P. A. *Angew. Chem., Int. Ed. Engl.* **1995**, *34*, 560.
(2) Concepción, P.; Corma, A.; Nieto, J. M. L.; Pérez-Pariente, J. *Appl. Catal. A* **1996**, *143*, 17.
(3) Dai, P. S. E.; Petty, R. H.; Ingram, C. W.; Szostak, R. *Appl. Catal. A* **1996**, *143*, 101.
(4) Thomas, J. M.; Raja, R.; Sankar, G.; Bell, R. G. *Acc. Chem. Res.* **2001**, *34*, 191.
(5) Iton, L. E.; Choi, I.; Desjardins, J. A.; Maroni, V. A. *Zeolites* **1989**, *9*, 535.
(6) Kurshev, V.; Kevan, L.; Parillo, D. J.; Pereira, C.; Kokotailo, G. T.; Gorte, R. J. *J. Phys. Chem.* **1994**, *98*, 10160.
(7) Lourenço, J. P.; Ribeiro, M. F.; Fibeiro, F. R.; Rocha, J.; Onida, B.; Garrone, E.; Gabelica, Z. *Zeolites* **1997**, *18*, 398.
(8) Hochtl, M.; Jentys, A.; Vinek, H. *Microporous Mesoporous Mater.* **1999**, *31*, 271.
(9) Barret, P. A.; Sankar, G.; Catlow, C. R. A.; Thomas, J. M. *J. Phys. Chem.* **1996**, *100*, 8977.
(10) Sponer, J.; Cejka, J.; Dedecek, J.; Wichterlová, B. *Microporous Mesoporous Mater.* **2000**, *37*, 117.
(11) Weckhuysen, B. M.; Rao, R. R.; Martens, J. A.; Schoonheydt, R. A. *Eur. J. Inorg. Chem.* **1999**, 565−577.
(12) Cundy, C. S.; Cox, P. A. *Chem. Rev.* **2003**, *103*, 663.
(13) Parise, J. B. *Stud. Surf. Sci. Catal.* **1985**, *24*, 271.
(14) He, H.; Long, Y. *J. Inclusion Phenomena* **1987**, *5*, 591.
(15) Simmen, A. Ph.D. Thesis, ETH, Zurich, Switzerland, 1992.
(16) Glasser, J. P.; Howie, R. A.; Kan, Q. B. *Acta Crystallogr.* **1984**, *C50*, 848.
(17) Chippindale, A. M.; Powell, A. V.; Jones, R. H.; Thomas, J. M.; Cheetham, A. K.; Huo, Q. S.; Xu, R. R. *Acta Crystallogr.* **1994**, *C50*, 1537.
(18) Kirchner, R. M.; Grosse-Kunstleve, R. W.; Pluth, J. J.; Wilson, S. T.; Broach, R. W.; Smith, J. V. *Microporous Mesoporous Mater.* **2000**, *39*, 319.
(19) Kongshaug, Q. O.; Fjellvag, H.; Klewe, B.; Lillerud, K. P. *Microporous Mesoporous Mater.* **2000**, *39*, 333.
(20) Baerlocher, Ch.; Meier, W. M.; Olson, D. H. *Atlas of Zeolite Structure Types*; Elsevier: Amsterdam, The Netherlands, 2001.
(21) Borges, C.; Ribeiro, M. F.; Fernandes, A.; Henriques, C.; Lourenço, J. P.; Rocha, J.; Gabelica, Z. Manuscript in preparation.
(22) Borges, C.; Ribeiro, M. F.; Henriques, C.; Lourenço, J. P.; Valange, S.; Louati, A.; Gabelica, Z.; Murphy, D. M. Manuscript in preparation.
(23) Treacy, M. M. J.; Higgins, J. B. *Collection of Simulated XRD Powder Patterns for Zeolites*; Elsevier: Amsterdam, The Netherlands, 2001.
(24) Borges, C. Ph.D. Thesis, IST, Lisbon, Portugal, 2003.
(25) Jorda, J. L.; McCusker, L. B.; Baerlocher, C.; Morais, C. M.; Rocha, J.; Fernandez, C.; Borges, C.; Lourenço, J. P.; Ribeiro, M. F.; Gabelica, Z. *Microporous Mesoporous Mater.* **2003**, *65*, 43.
(26) McCusker, L. B. Personal communication.
(27) Verberckmoes, A. A.; Weckhuysen, B. M.; Schoonheydt, R. A. *Microporous Mesoporous Mater.* **1998**, *22*, 165.
(28) Schoonheydt, R. A.; De Vos, R.; Pelgrims, J.; Leeman, H. *Stud. Surf. Sci. Catal.* **1989**, *49*, 559.
(29) Marchese, L.; Chen, J.; Thomas, J. M.; Collucia, S.; Zecchina, A. *J. Phys. Chem.* **1994**, *98*, 13350.
(30) Barret, P. A.; Sankar, G.; Catlow, C. R. A.; Thomas, J. M. *J. Phys. Chem.* **1996**, *100*, 8977.
(31) Berndt, H.; Martin, A.; Zhang, Y. *Microporous Mater.* **1996**, *6*, 1.
(32) Weckhuysen, B. M.; Verberckmoes, A. V.; Uytterhoeven, M. G.; Mabbs, F. E.; Collison, D.; de Boer, E.; Schoonheydt, R. A. *J. Phys. Chem. B* **2000**, *104*, 37.
(33) Thomson, S.; Luco, V.; Howe, R. *Phys. Chem. Chem. Phys.* **1999**, *1*, 615.
(34) Lee, Y. J.; Chon, H. *J. Chem. Soc., Faraday Trans.* **1996**, *92*, 3453.
(35) Banci, L.; Bencini, A.; Benelli, C.; Gatteschi, D.; Zanchini, C. *Struct. Bonding* **1982**, *52*, 37.
(36) Pilbrow, J. R. *Transition Ion Electron Paramagnetic Resonance*; Oxford Science Publications: Oxford, UK, 1990; p 150.
(37) Makinen, M. W.; Kuo, L. C.; Yim, M. B.; Wells, G. B.; Fukuyama, J. M.; Kim, J. E. *J. Am. Chem. Soc.* **1985**, *107*, 5245.
(38) Colluccia, S.; Marchese, L.; Martra, G. *Microporous Mesoporous Mater.* **1999**, *30*, 43.
(39) Kazansky, V. B. *Catal. Today* **1988**, *3*, 367.
(40) Dellepiane, G.; Zerbi, G. *J. Chem. Phys.* **1968**, *48*, 3573.
(41) Su, B. L.; Norberg, V. *Langmuir* **2000**, *16*, 6020.
(42) Hadjiivanov, K.; Saussey, J.; Freysz, J.-L.; Lavalley, J.-C. *Catal. Lett.* **1998**, *52*, 525.
(43) Hadjiivanov, K.; Tsyntsarski, B.; Nikolova, T. *Phys. Chem. Chem. Phys.* **1999**, *1*, 4521.
(44) Gianotti, E.; Marchese, L.; Martra, G.; Coluccia, S. *Catal. Today* **1999**, *54*, 547.
(45) Li, Y.; Slager, T. L.; Armor, J. N. *J. Catal.* **1994**, *150*, 376.
(46) Li, Y.; Armor, J. N. *J. Catal.* **1994**, *150*, 388.
(47) Hadjiivanov, K. *Catal. Rev.-Sci. Eng.* **2000**, *42*, 71.
(48) Costa, C. S.; Lourenço, J. P.; Henriques, C.; Antunes, A. P.; Ribeiro, F. R.; Ribeiro, F. M.; Gabelica, Z. *Proceedings of the 12th International Zeolite Conference*; Treacy, M. M. J., Marcus, B. K., Bisher, M. E., Higgins, J. B., Eds.; Materials Research Society: Warrendale, 1999; p 1771.
(49) Dumont, N.; Gabelica, Z.; Derouane, E. G.; McCusker, L. B. *Microporous Mater.* **1993**, *1*, 149.
(50) Gabelica, Z.; Louati, A.; Borges, C.; Ribeiro, M. F.; Lourenço, J. P.; Murphy, D. M.; *Proceedings of the 14th International Zeolite Conference* [CD-ROM]; van Steen, E. W. J., Callanan, L. H., Claeys, M., O'Connor, C. T., Eds.; Capetown, 2004; Vol. 1, p 1649.
(51) Rolison, D. R. *Chem. Rev.* **1990**, *90*, 867.
(52) Brendle, E.; Louati, A. *Electroanalysis* **2000**, *12*, 1147.